Influence of Welding Pressure on Diffusion Welded Joints Using Interlayer

Considering diffusion welding for superior performances

BY G. THIRUNAVUKARASU, B. MURUGAN, S. CHATTERJEE, AND S. KUNDU

ABSTRACT

The present study focused on elucidating the extent of influence of welding pressure on the evolution of interfacial microstructure, mechanical properties, and fracture morphologies of solid-state diffusion-welded joints (DWJs) of Ti-6Al-4V (TiA) and 304 stainless steel (SS) using 200-µm-thick nickel (Ni) as an interlayer processed in vacuum at 750°C for 60 min using welding pressure in the range of 2 to 10 MPa in step of 2 MPa. Layer wise Ni–Ti-based intermetallic phase(s) were revealed at the TiA|Ni interface, whereas the Ni|SS interface showed solid solution behavior. From the surface property of the DWJs, it was sensed that the effect of work hardening occurred when the welding was processed at 4 MPa and above welding pressures. Exponential growth in the bulging property of the DWJs with the increase in the welding pressure was spotted. The study indicated the significant influence of welding pressure over the welded assemblies' tensile properties; however, tensile properties behaved asymptotic when the DWJs were processed beyond 6-MPa welding pressure. To understand the fracture characteristic of the DWJs, fracture path and fractography were evaluated. Thermal stresses induced on the materials diffusion welded were calculated.

KEYWORDS

• Diffusion Welding • Ti Alloys • Stainless Steels • Intermetallics
• Mechanical Properties

Introduction

Diffusion welding (DW) is a high-temperature solid-state joining process that permanently joins mating surfaces by simultaneous application of pressure and heat. It does not involve macroscopic deformation, melting, or relative motion of the parts welded. A solid filler metal (diffusion aid) may be inserted between the faying surfaces (Ref. 1). DW has demonstrated its uniqueness by finding application in the processes and products of front line areas of science and technology. DW is actually gaining momentum of applicability from the days of conception due to the inappropriateness of other joining techniques.

In the past quarter-century, Ti alloys have been successfully used in aircrafts, rockets, and biomedical implants, among other products, as key structural materials. Ti alloys derive their excellent properties from a combination of two ductile phases (hcp and bcc allotropic modifications) of Ti. Several key features of these phases independently and dependently determine the plasticity and fracture behavior of the family of Ti-alloys (Ref. 2). Both the high corrosion resistance and the good strength/weight ratios of titanium and its family of alloys make them an attractive prospect for use in offshore oil and gas platforms. Ti-alloy armor is being incorporated into the design of some combat vehicles in order to save weight (Ref. 3).

Although Ti alloys are nonmagnetic, their high electrical resistivity is used in the manufacture of electromagnetic cookware. In addition to the capability of electromagnetic cooking, titanium's light weight, low heating capacity, and good corrosion resistance are the favorable properties of these cookwares (Ref. 4).

Austenitic stainless steels (ASSs) are the most common and familiar type of stainless steels. They are recognized as nonmagnetic. They are extremely formable and weldable, and successfully used from cryogenic to red-hot temperatures. ASSs have exceptional toughness and a combination of strength and corrosion resistance at elevated temperatures. ASSs are the most creep resistant of the stainless steels. Lean austenitic alloys constitute the largest portion of all stainkess steels (SSs) produced. These are principally 201, 301, and 304 grades. Alloys with less than 20% Cr and 14% Ni fall into this unofficial category (Ref. 5). Highly efficient and reliable joints of corrosion-resisting-steels with titanium alloys find the greatest inevitable need in nuclear power engineering (Ref. 6).

In a satellite cooling system, Ti-6Al-4V is joined to stainless steel

G. THIRUNAVUKARASU, B. MURUGAN, S. CHATTERJEE, and S. KUNDU (skundu@metal.iiests.ac.in) *are with the Department of Metallurgy and Materials Engineering, Indian Institute of Engineering Science and Technology, Shibpur, India.*

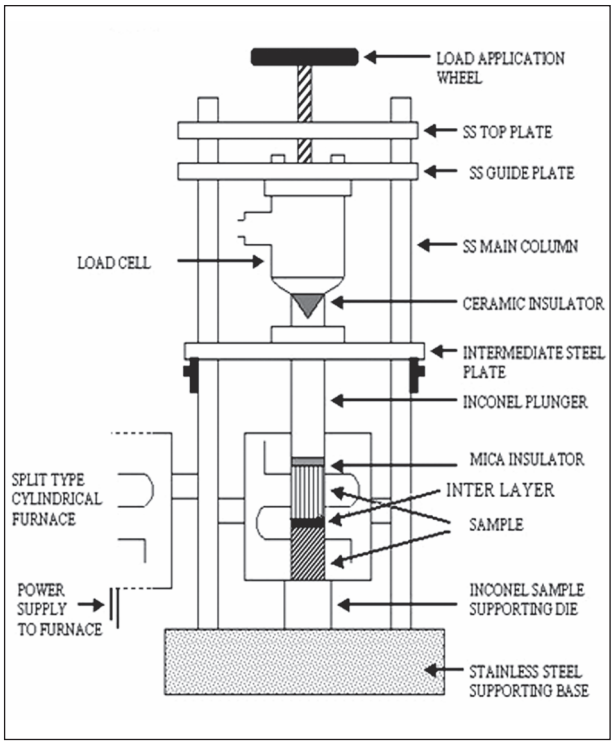

Fig. 1 — Schematic diagram of the indigenous fixture used for processing DWJs.

(1Cr18Ni9Ti) (Ref. 7). Joints of Ti alloy and Type 304 ASS are used in fuel tanks of satellite launch vehicles (Ref. 8); hence, joints of Ti-based alloy and SS using different welding techniques are undertaken as sponsored research by different agencies and institutes to know the details of optimal levels of operating parameters to achieve far better performance.

Table 1 shows the physical properties of Ti-6Al-4V and 304 SS (Ref. 9). It is readily seen that large property differences exist between the metals. The large variation of these and other properties provide an attractive source for the choice of materials for special service conditions and environments; however, the large differences in physical properties also yield difficulties in joining these metals together. A large difference in the melting temperature between two metals makes the conventional fusion-welding processes inapplicable due to the segregation of low-melting eutectics, which can cause hot cracking. Large differences in thermal expansion will lead to the formation of large residual stresses and this leads to the formation of microcracks at the welded region; and thus reduce the joint strength and cause fatigue problems. A difference in the thermal conductivity of two metals easily causes uneven heat dissipation. Furthermore, chemical mismatches in dissimilar-metal joints can result in the formation of brittle phases and the diffusion of particular elements. These will adversely affect the service properties of the joints, and are the main reasons why dissimilar-metal joining is normally more complex than similar-metal joining in many respects. Consequently, a solid-state joining method, viz., DW of these two materials using an interlayer, has gained more importance than other conventional welding methodologies. During welding, Ti alloys pick up oxygen and nitrogen from the atmosphere very easily (Refs. 10, 11). For this reason, DW in a vacuum or inert gas atmosphere is suggested.

One of the necessary conditions to considering a material as a potential interlayer to join the base metal(s) is that it reduces the chemical heterogeneity and improves the thermodynamic stability of the diffusion zone at the interface of the welded joints. Zeer et al. (Ref. 12) proposed a method to classify interlayers for DW of dissimilar materials and discussed the role and contribution of the interlayers in the formation of the diffusion welded joints (DWJs) in different stages of welding. They advised using interlayers made from alloys or pure metals, usually with high ductility, such as nickel, copper, cobalt, zirconium, vanadium, Permalloy, silver and gold. The interlayers were used in the form of foil, film, or coatings and deposited on one or both sides of the to-be-welded surfaces by electroplating or thermal spraying, rolling of powders, and in the combined form of spraying and foil. Nickel was considered as a potential candidate for the interlayer due to its corrosion resistance for application at high temperature and substantial solid solubility with iron. Ni–Ti binary phase diagram suggested that intermetallics formation changes from $NiTi_2$ to Ni_3Ti via NiTi with increasing Ni (Refs. 13, 14). He et al. (Ref. 15) reported Ni–Ti intermetallics have higher plasticity than Fe–Ti intermetallics.

The success or failure of the DW process depends on welding pressure, temperature, and time (Ref. 16). In the past, most literature reported either the effect of temperature or time on the DWJs' microstructure and mechanical properties. The present authors along with Professor Mishra carried out two separate investigations on DWJs of TiA and SS using 200-µm-thick Ni as an interlayer. To first optimize the welding temperature (Ref. 17), DWJs were prepared in the temperature range from 700° to 800°C in steps of 25°C using 3-MPa pressure for 60 min. A maximum tensile strength of ~206 MPa along with a ductility of ~2.9% was obtained for the DWJs processed at 750°C. Secondly, to optimize the welding time (Ref. 18), DWJs were processed using 4-MPa pressure at 750°C by varying the time from 30 to 120 min in steps of 15 min. Maximum tensile strength of ~382 MPa along with elongation of ~3.7% was observed for the DWJs processed for 60 min. Although it is universally accepted that welding pressure is a very important variable in the solid-state DW process, up until now there existed no sufficient, well-established empirical study/proof to back up such a hypothesis.

In view of limited studies, the present research work described in this pa-

Table 1 — Physical Properties of Base Metals

Metal	Melting Point (°C)	Density (g/cc)	Thermal Conductivity (W/m–K)	Coefficient of Thermal Expansion (µm/m–°C), linear 250°C
304 SS	1400–1455	8	16.2	17.8
Ti-6Al-4V	1604–1660	4.43	6.7	9.2

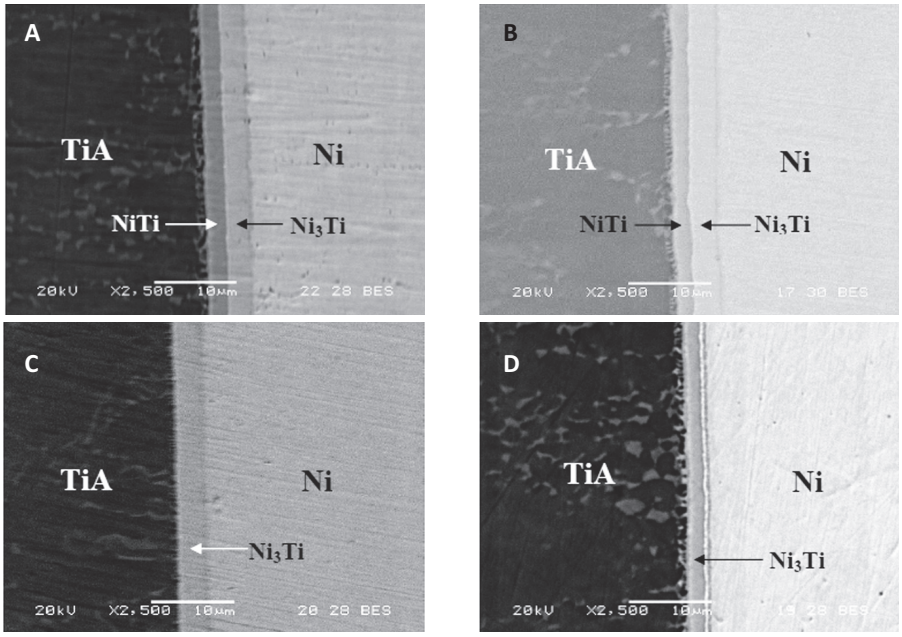

Fig. 2 — SEM-BSE images of TiA|Ni interface of DWJs processed at 750°C for 60 min using A — 2 MPa; B — 4 MPa; C — 6 MPa; D — 8 MP.

per was undertaken by the researchers in an attempt to know the extent of significant influence of pressure variation over intermetallics formation at the diffusion zone, the lateral plastic deformation, the room-temperature mechanical properties (tensile properties and hardness), and the fracture geographies of DWJs and to provide information about the possible causes. As this work is in continuation of the previous works (Refs. 17, 18), the optimized temperature of 750°C and the optimized time of 60 min were chosen from the respective literature sources (Refs. 17, 18). Choosing higher welding temperature and longer welding time deteriorated the DWJs' strength due to the formation of a large volume of Ni–Ti-based intermetallics at the TiA|Ni interface (Refs. 17, 18). Even higher temperature and longer time will lead to the formation of Fe–Ti-based intermetallics that are more detrimental to the mechanical properties of the DWJs. Herein, the experimental investigation of influence of welding pressure on the evolution of interfacial microstructure and the mechanical properties of solid-state diffusion welded joints of Ti-6Al-4V (TiA) and 304 stainless steel (SS) using 200-μm-thick Ni as an interlayer was processed in vacuum at 750°C (welding temperature) for 60 min (welding time) using welding pressure in the range of 2 to 10 MPa in steps of 2 MPa.

Experimental Procedures

Base metals: Ti-6Al-4V wt-% [a.k.a. TiA] and Fe-18Cr-8Ni wt-% [a.k.a. SS] and interlayer: 99.5 wt-% Ni (~200 ± 10 μm), were used in this investigation. Mating surfaces of base metals and interlayer were polished using diamond paste (1 μm) after grinding by hand using eleven series of SiC emery papers (grit sizes 40# to 1600#) to reduce surface roughness. Before DW, the mating surfaces were cleaned with acetone and dried using a portable hair dryer. In this study, DWJs were processed using a special fixture (Fig. 1) designed and manufactured indigenously. The fixture design is capable of processing only one DW experiment at a given point in time; hence, the DW experiments are time consuming by nature and by design. Mica of ~1-mm thick was kept on the supporting die (Inconel) of the fixture — Fig. 1. The TiA|Ni|SS assembly was placed over the mica. Mica avoids the interfacial contact between the assembly and the supporting die. Over the assembly, mica was again placed to avoid the interfacial welding between the plunger (Inconel) and the assembly. A ceramic-type insulator was used in between load cell and plunger to prevent metal-metal contact. Over the load cell, screw threaded wheel (of stainless steel) for load application was mounted. After positioning all the above items in-line, a load cell (capacity: 500 kg) was connected to the load indicator, and the required welding pressure (2–10 MPa) was applied along the centerline of the assembly using the threaded wheel that acts over the load cell and the to-be-diffusion-welded assembly. This threaded wheel is used to control the welding pressure applied on the assembly. The welding pressure applied was measured at room temperature. The fixture with the assembly was inserted inside a vacuum chamber, with one end of the vacuum chamber sealed using nuts and bolts and the other end connected to a vacuum unit. After reaching enough vacuum (~6–8 × 10^{-3} Pa), temperature was increased from 32°C (room temperature) to 750°C (welding temperature) at the rate of 0.24°Cs^{-1}. The TiA|Ni|SS assemblies were held for 60 min (welding interval) at 750°C. Power supply to the welding furnace was switched off after 60 min. At each level of the welding pressure factor, three separate experiments were conducted to process three samples of DWJs.

In this study, experiments were performed at five different levels (2, 4, 6, 8, and 10 MPa) of welding pressure factor; hence, there are a total of 15 individual, independent, and random experiments (three experiments repeated at each level of the welding-pressure factor).

After the DW process, DWJs were sectioned perpendicular to the mating surface and the surfaces were prepared by metallurgical polishing techniques. Polished surfaces of DWJs were examined in an SEM (JSM-5510, JEOL) in backscattered electron mode (SEM-BSE) to obtain finer microstructural features of diffusion zone. Chemical composition of the reaction layers were determined by energy dispersive spectroscopy (SEM-EDS, Thermo Electron Corporation-Noran System Six C10018) using a SiLi detector. Tensile properties of DWJs were evaluated with an Instron 4204 at a cross-head speed of 8.33 × 10^{-4} mms^{-1}. Cylindrical tensile specimens (gauge diameter: 4 mm, gauge length: 20 mm) were machined as per ASTM specification E8M-11 (Ref. 19). The average of the tensile properties of three DWJs processed at each pressure level along with the associated errors were reported here.

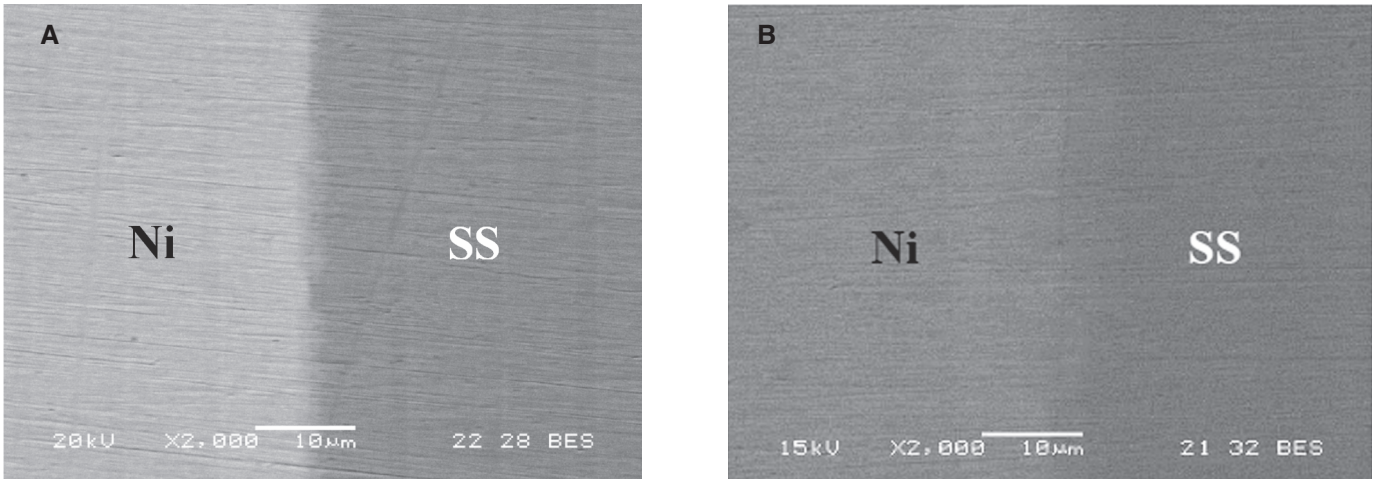

Fig. 3 — SEM-BSE images of Ni|SS of DWJs processed using welding pressure of A — 2 MPa; B — 10 MPa.

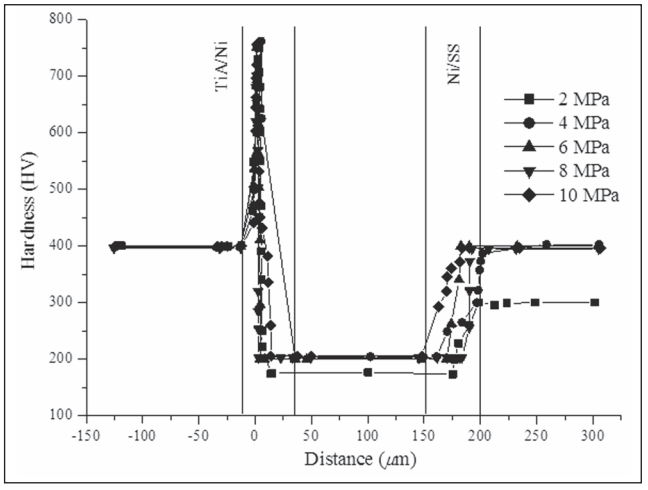

Fig. 4 — Microhardness profile along the interfaces of DWJs processed using various welding pressures.

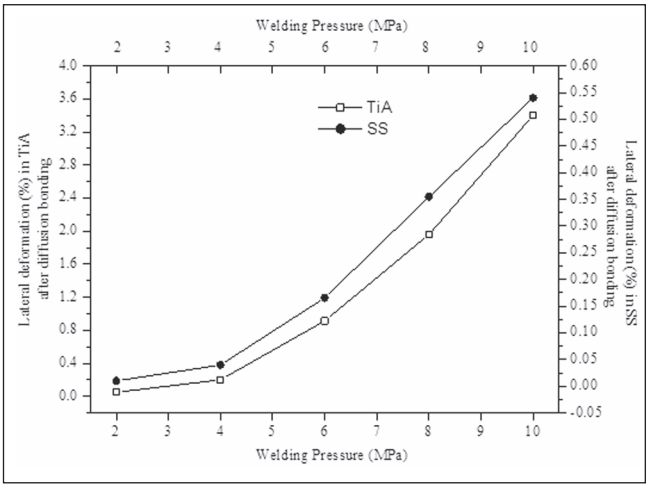

Fig. 5 — Variation of lateral deformation (%) in TiA and SS of DWJs with respect to the welding pressure applied.

Microhardness measurements were carried out on the polished surface of DWJs using Vickers diamond indenter (Leica VMHT) with a load of 25 gram force for 20 s dwelling time. Five measurements were carried out at each section and the respective average was mentioned in this study. Fracture surfaces of DWJs were observed in secondary electron mode using the SEM-EDS to reveal the nature and most possible location through which failure was initiated during tensile loading. SEM-BSE observations were also made to study the location of the fracture path, while fractography examination was carried out using secondary electrons of SEM.

Results

Absence of discontinuities and voids at both the interfaces (both TiA | Ni and Ni | SS in Figs. 2, 3, respectively) was revealed, which established the superior contact of the mating surfaces with process parameters; hence, DWJs were efficacious. Layer wise intermetallics were observed at the TiA | Ni interface (Fig. 2), whereas the Ni | SS interface (Fig. 3) revealed solid-solution behavior. It was observed that the TiA | Ni interfaces (Fig. 2) of the DWJs processed using 6 and 8 MPa had only a light-shaded reaction layer. The light-shaded reaction layer on an average consisted of Ti (~27 at.-%) and Ni (~70 at.-%); hence, the Ni–Ti binary phase diagram indicated the realization of Ni_3Ti intermetallic (Refs. 13, 14).

The TiA | Ni interface of the DWJs processed using 2, 4, and 10 MPa had two reaction layers. The deep-shaded reaction layer observed adjacent to the TiA matrix consisted of Ti (~50 at.-%) and Ni (~45 at.-%); hence, the Ni–Ti phase diagram indicated the possibility of realization of NiTi intermetallic (Refs. 13, 14). The reaction layer adjacent to the Ni matrix was light shaded Ni_3Ti intermetallic. In general, for all DWJs, the width of Ni_3Ti intermetallic was wider compared to the NiTi intermetallic at the reaction zone (Ref. 18). The formation of the similar Ni–Ti-based reaction products were also observed in the literature (Refs. 20, 21).

It was observed, the hardness of the TiA side (Fig. 4) of the DWJs was ~400 HV irrespective of the welding pressure adopted during the experiments. The hardness of the other base metal side (SS side) of the DWJs was witnessed to be ~300 HV for the DWJs processed at 2 MPa, whereas the surface hardness of the SS side was ~400 HV for the DWJs processed from

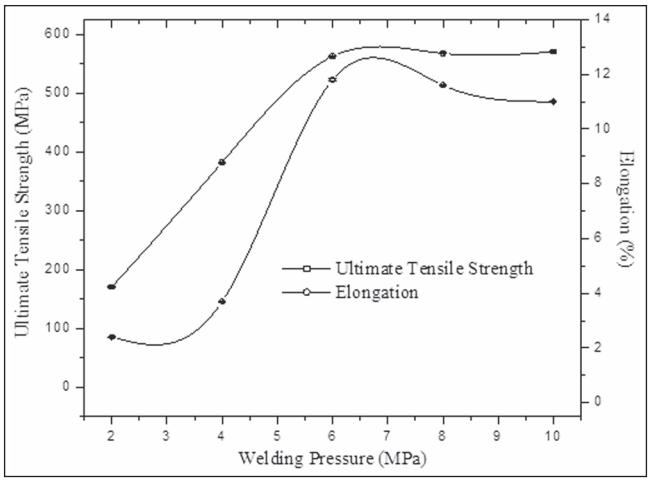

Fig. 6 — Tensile strength (MPa) and breaking strain (%) of DWJs processed at different levels of welding pressure.

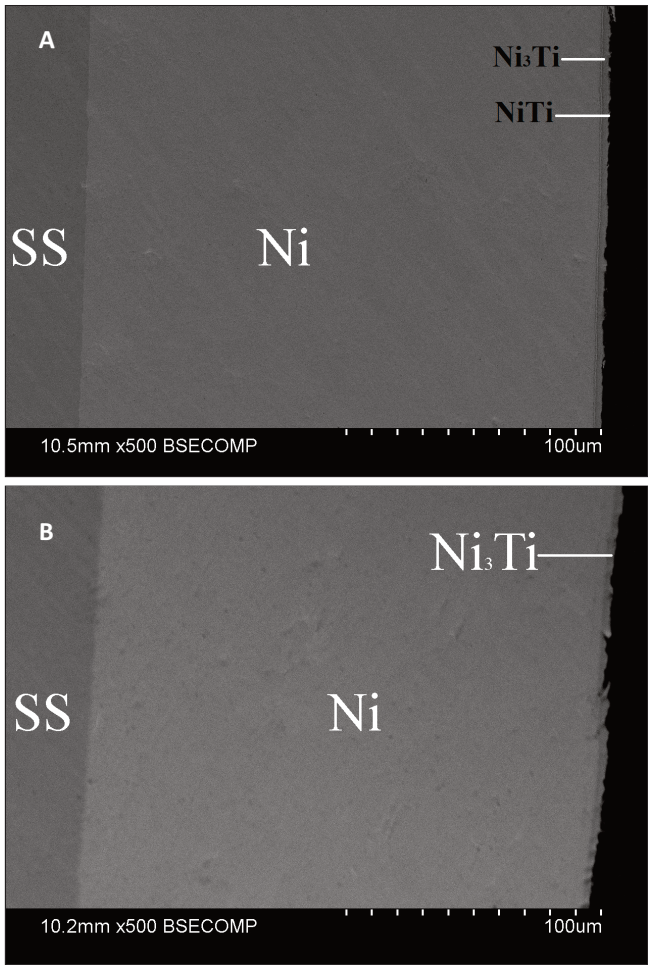

Fig. 7 — Fracture path of DWJs processed at A — 2 MPa—SS side; B — 6 MPa—SS side.

4 to 10 MPa. In the same way, the hardness of the interlayer zone (Ni) of the DWJs was found to be ~175 HV for the DWJs processed at 2 MPa, whereas it was ~200 HV for the DWJs processed from 4 to 10 MPa. It was observed that the increase in the welding pressure had a significant influence in increasing the bulk property (hardness) of the SS side and Ni zone but such phenomenon was not observed in the case of the TiA-side.

The materials that were diffusion welded underwent serious changes in shape, i.e., geometry. In reality, whenever a force is applied to a solid object, a stress is produced within the object. The physical effect/manifestation of this stress is that the object experiences some form and amount of deformation, a strain. As the DWJs were prepared at five different levels of the welding-pressure factor, it was decided to observe the lateral deformation of the DWJs. The lateral deformation (Equation 1) of the DWJs is defined as follows:

$$\text{Lateral deformation (\%)} = \frac{(d_2 - d_1)}{d_1} \times 100 \qquad (1)$$

d_1: (diameter of base metal section) $_{\text{before diffusion-bonding}}$

d_2: (diameter of base metal section) $_{\text{after diffusion-bonding}}$

The details of the lateral deformation of TiA and SS are given in Fig. 5. The lateral deformation of the TiA side of the DWJs was much higher than that of the lateral deformation of the SS side of the respective DWJs. The reason for the significant differences in the lateral deformation of TiA side and SS side needs to be figured out.

Both tensile strength and elongation (Fig. 6) increased with the increase in the welding pressure from 2 to 6 MPa. Increase in the strength and elongation of the DWJs with the increase in pressure was presumably due to the improvement in the coalescence of the mating surfaces of the DWJs. There was no significant difference in the tensile strength of DWJs processed above 6 MPa. The tensile curve was more or less flat for the DWJs processed above 6 MPa. Elongation dropped insignificantly for the DWJs processed above 6 MPa. A slight drop in the elongation of DWJs with the increase in the welding pressure from 6 to 10 MPa is due to the work hardening effect (Ref. 22) experienced by DWJs. DWJs processed at 6 MPa achieved the optimal strength of ~560 MPa with substantial elongation of ~12 %. In this work, dissimilar metal joints of Ti-6Al-4V and 304 SS achieved the highest strength of ~560 MPa, which is also the best performance of the joints processed to date in other routes reported in literature (Refs. 23–29). Shanmugarajan et al. (Ref. 23) achieved ~40 MPa for the laser welded joints of Ti and SS using Ta as an interlayer. Wang et al. (Ref. 24) were able to reach ~124 and ~234 MPa for the electron beam welding of titanium alloy to SS using Ni and Cu filler metal, respectively. Balasubramanian (Refs. 25, 26) achieved ~158 MPa for DWJs of Ti-6Al-4V and 304 SS using an Ag interlayer. Tomashchuk et al. (Ref. 27) reached ~350 MPa for electron beam welded joints of Ti alloy and SS via copper as interlayer. Norouzi et al. (Ref. 28) achieved ~374 MPa for transient liquid phase (TLP) welded joints of Ti-6Al-4V and AISI 304 austenitic SS using Cu interlayer. Kumar et al. (Ref. 29) accomplished the highest tensile strength of ~523 MPa for the dissimilar metal joints of Ti-6Al-4V and SS304L with Cu as interlayer through friction welding technique. This work proved DW is a promising route to process dissimilar metal joints with far better mechanical properties.

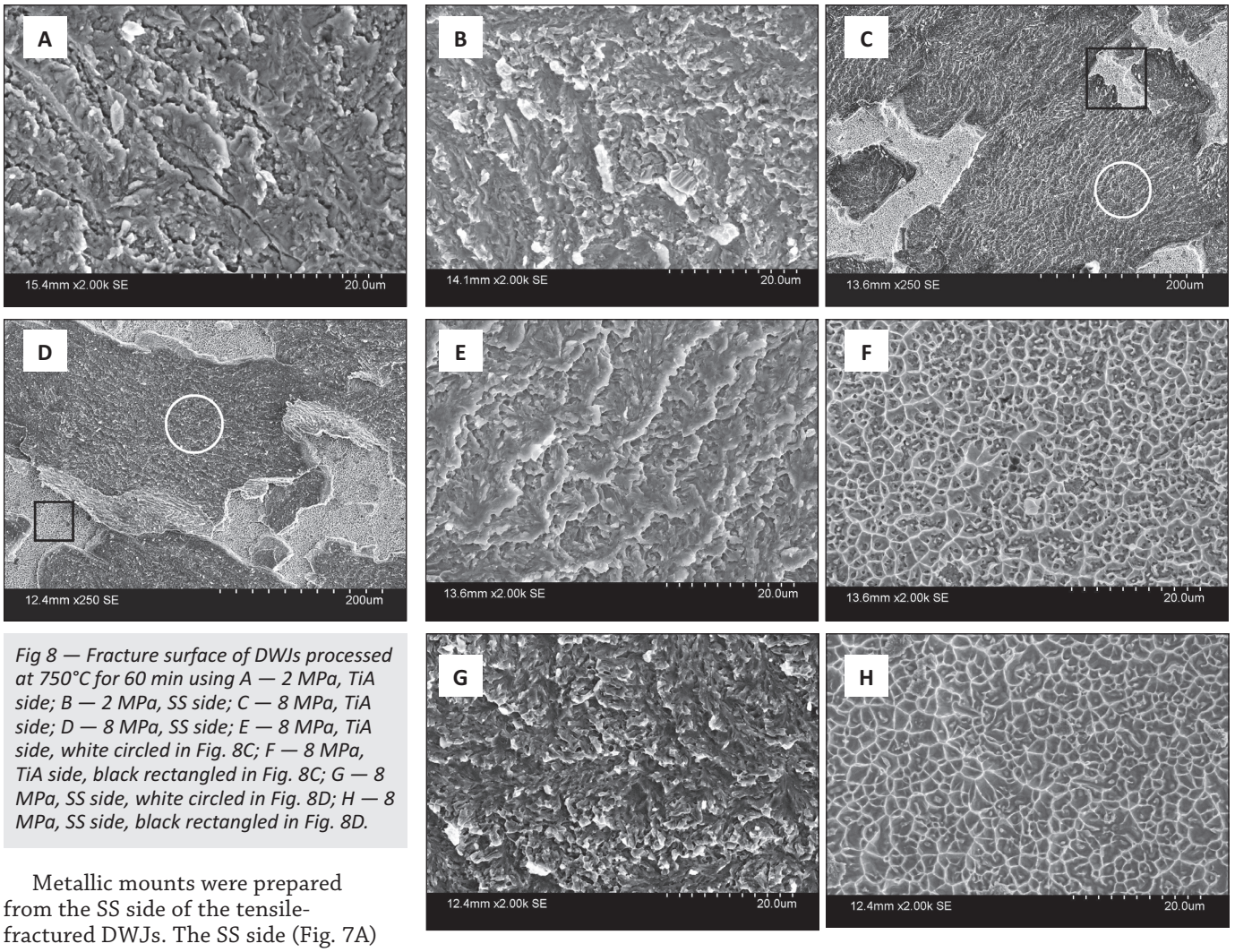

Fig 8 — Fracture surface of DWJs processed at 750°C for 60 min using A — 2 MPa, TiA side; B — 2 MPa, SS side; C — 8 MPa, TiA side; D — 8 MPa, SS side; E — 8 MPa, TiA side, white circled in Fig. 8C; F — 8 MPa, TiA side, black rectangled in Fig. 8C; G — 8 MPa, SS side, white circled in Fig. 8D; H — 8 MPa, SS side, black rectangled in Fig. 8D.

Metallic mounts were prepared from the SS side of the tensile-fractured DWJs. The SS side (Fig. 7A) of the fractured DWJ processed at 2 MPa revealed ample Ni interlayer; hence, the SEM micrographs of the metallic mounts suggested that the lower welding pressure functionally favored the fracture along the TiA | Ni interface with the intermetallics (Ni_3Ti and NiTi) completely cleaved off the TiA matrix. The fracture path (Fig. 7B) of the DWJ processed using 6 MPa exposed the full length of the Ni layer. It was observed that the DWJ processed using 6 MPa had proofs of Ni_3Ti intermetallic attached to the edge of Ni foil; therefore, the electron micrographs of the metallic mounts recommended that DWJs processed at higher welding pressure also preferred to fracture along the TiA | Ni interface with the intermetallic (Ni_3Ti) completely hewed off the TiA matrix. In brief, the fracture path (Fig. 7) observation yielded valuable information that the TiA | Ni | SS DWJs fractured along the TiA | Ni interface regardless of the welding pressure chosen.

Selective tensile fractured samples along the TiA side and SS side of DWJs processed at 2 and 8 MPa were shown in Fig. 8. Both the fracture features of the TiA side (Fig. 8A) and SS side (Fig. 8B) of DWJ processed at 2 MPa did not show any sign of dimpled-rupture (ductile) mode of failure; but showed the noted "river marks." Both the fractographs (Figs. 8A and B) had typical slightly faceted appearances principally because of the changes in the orientation of the cleavage planes operating from grain to grain; hence, it was established that the DWJs processed at 2 MPa had undergone a majorly brittle fracture of intergranular mode apparently through the TiA | Ni interface during tensile loading.

Both the fracture structures of the TiA side (Fig. 8C) and SS side (Fig. 8D) of the DWJ processed at 8 MPa detected two distinct regions. Firstly, the zones identified as white circles were faceted river-pattern rupture (brittle) mode of failure; secondly, the zones identified using black rectangles were dimpled-rupture (ductile) mode of failure. Although the faceted river patterns were more in volume as compared to the other feature in the fractographs (Figs. 8C and D), it could be comfortably claimed that the DWJs processed using 8 MPa had undergone a mixed mode of failure. For better visualization and understanding, the details of the zone identified as white circles in Figs. 8C and D were shown in Figs. 8E and G, respectively. Similarly, the details of the zone identified as black rectangles in Figs. 8C and D were shown in Figs. 8F and H, respectively. In general, it was learned that the lowest welding pressure (2 MPa) yielded brittle fracture morphologies; and finally, the higher welding pressure (8 MPa) yielded mixed mode fractural features.

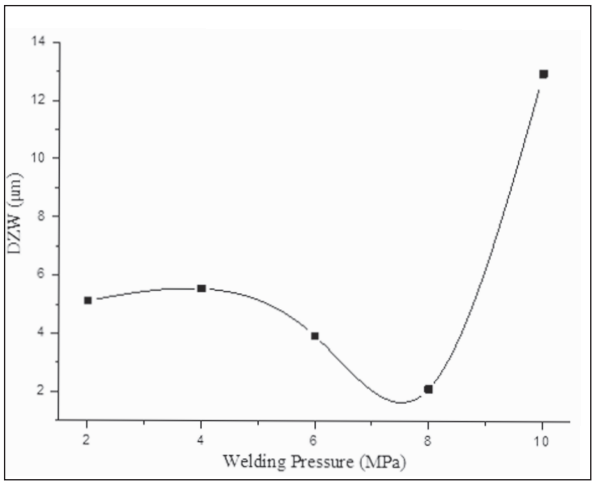

Fig. 9 — Diffusion zone width (DZW) at TiA|Ni interface of DWJs processed at different welding pressures.

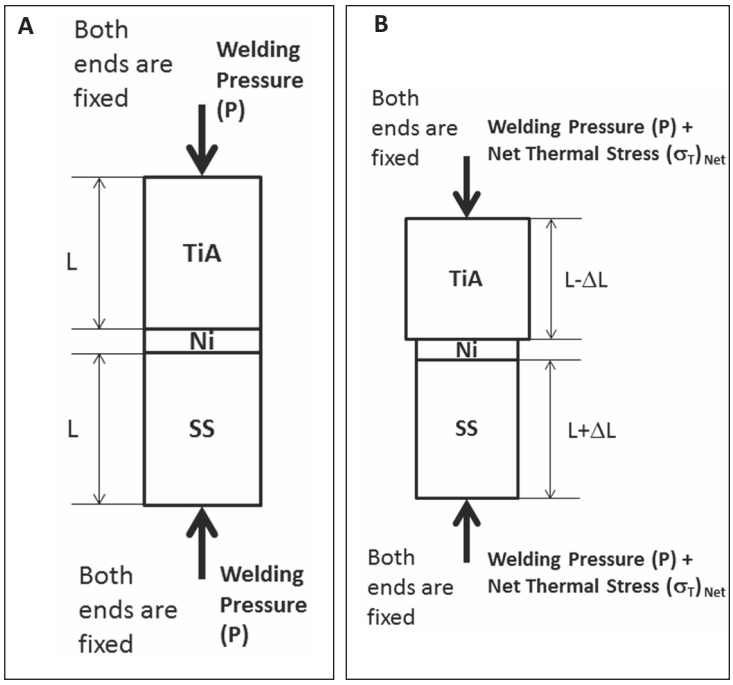

Fig. 10 — Line sketch of the materials assembled in the DW fixture when furnace temperature was at A — 32°C (ambient temperature); B — 750°C (welding temperature).

Discussion

Sensible reasons for the presence of the layer-wise Ni–Ti-based intermetallics at the TiA|Ni interface and the solid-solution behavior at the Ni|SS interface could be explained using Hume-Rothery rules and the principle of electronegativity (Ref. 18). At the interfaces, the atoms from both sides diffuse in the opposite direction, but there is an effective diffusion of atoms at each interface that is more predominant than the other direction. At the TiA|Ni interface, Ni atoms diffused deeper into the TiA matrix as compared to the diffusing capability of Ti atoms into the Ni matrix. Similarly, net flux of Ni atoms past the interface in one direction were faster than the flux of atoms in SS in the opposite direction; hence, the effect proposed by Kirkendall was observed at Ni|SS interface for all DWJs (Ref. 18).

As DWJs fractured at the TiA|Ni interface due to the presence of intermetallics at the interfacial reaction (diffusion) zone, the diffusion zone width (DZW) of the TiA|Ni interface was measured. The DZW (Fig. 9) at the interface of the DWJs processed at 2 and 4 MPa have negligible significant differences. The DZW decreased with the increase in the welding pressure from 4 to 8 MPa. The DZW increased with the increase in the welding pressure from 8 to 10 MPa. A decrease in the DZW with an increase in the welding pressure, from 4 to 8 MPa, indicated there was a decrease in the net activity (diffusivity) of atoms at the TiA|Ni interfaces. A decrease in the net activity of atoms with an increase in welding pressure shows an inverse relationship.

Most of our engineering materials are polycrystalline so that grain boundary diffusion is far more important than surface diffusion. Deformation forces the dislocations that exist in a polycrystalline metal to move up and pile up at the grain boundaries, and new dislocations to be generated. Consequently, the increase in pressure hinders the grain boundary diffusion, which affects the surface diffusion phenomenon. Hence, interfacial activity was affected (Refs. 30–32). At 10 MPa, diffusion along the free surfaces is a dominant diffusion path. A free surface is associated with more open structure, and experiments showed that the jump frequency for atoms diffusing along this defect is higher than for diffusion in lattice and grain boundaries (Ref. 31). With an increase in the welding pressure to 10 MPa, effective free surface for contact of the mating surfaces was increased, thus the effective atomic mobility increased. Hence, DZW increases with welding pressure from 8 to 10 MPa.

The increase in the hardness of the Ni and SS with the increase in welding pressure could be attributed to the effect of work hardening. When material is deformed, work hardening occurs resulting in an increase in the hardness of the material. In general, the rate of work hardening is lower for hcp metals than for cubic metals. TiA is being hcp metal whereas that of Ni and SS are cubic metals. The hardness of Ni and SS were increased significantly with the increase in the welding pressure from 2 to 4 MPa and above, while the hardness of TiA (hcp metal) doesn't change with the welding pressure (Ref. 33). Along the Ni|SS interface, the hardness increased from Ni to SS and the observed hardness was ~220 HV for the DWJs processed at 2 MPa, whereas it was ~330 HV for 4 MPa and above welding pressures. Along the TiA|Ni diffusion zone, the hardness increased initially till it reached a maximum value and dropped toward Ni. The hardness of NiTi intermetallic and Ni_3Ti intermetallic was ~550 and ~750 HV, respectively. The hardness at NiTi/Ni_3Ti interface was ~650 HV. It was also noticed that the fracture was expected to occur apparently near the TiA|Ni interface because the hardness at the TiA|Ni interface (~750 HV) was much higher than the hardness at the Ni|SS interface (~330 HV), thus the TiA|Ni interface was more brittle as compared to the Ni|SS interface. Sam et al. (Ref. 19) in their study demonstrated that

DWJs failed through the TiA | Ni-alloy interface.

Here, the lateral deformation of the metals diffusion welded was of inelastic-type (plastic deformation); however, the plastic deformation of materials can be correlated with the elastic properties of the respective materials. There are three elastic moduli that derive from the spatial tri-dimensionality of the world. The three elastic moduli represent linear, planar, and volume effects on material. They are A) Young's modulus (E) [resistance to changes in length]; B) shear modulus (G) [resistance to transverse shift]; and C) bulk modulus (K) [resistance to compression or expansion]. Apart from these elastic moduli, there is another property called Poisson's ratio (μ) defined as the ratio of the transverse to the axial strain. These elastic moduli are generally anisotropic in the case of single crystals but, since the engineer usually works with polycrystalline materials in which the individual crystallites are arranged randomly, it can generally be assumed that the mechanical properties of materials are isotropic (Refs. 34–36). Although change in volume is related to the bulk modulus (K) property of the material, it can be related to the other elastic moduli using the following relationships (Equations 2 and 3) (Ref. 36):

$$E=3K(1-2\mu) \quad (2)$$

$$E=2G(1+\mu) \quad (3)$$

Using Equations 2 and 3, it could be perceived that Young's modulus of materials could explain the potential causes for significant differences in the lateral (plastic) deformation of the TiA and SS sides of the DWJs. The elastic (Young's) modulus of Ti-alloy (Ti-6Al-4V) and austenitic stainless steels (304 SS) is ~120 GPa (Ref. 3) and ~198 GPa (Ref. 37), respectively. As Young's modulus of Ti-6Al-4V is much lower as compared to Young's modulus of 304 SS, the TiA side of DWJs underwent an excess amount of lateral deformation as compared to the SS side of the respective DWJs; hence, it could be stated that the lateral deformation of the material is inversely proportional to its elastic modulus (Equation 4).

$$\text{Lateral deformation} \propto \frac{1}{\text{Elastic modulus}} \quad (4)$$

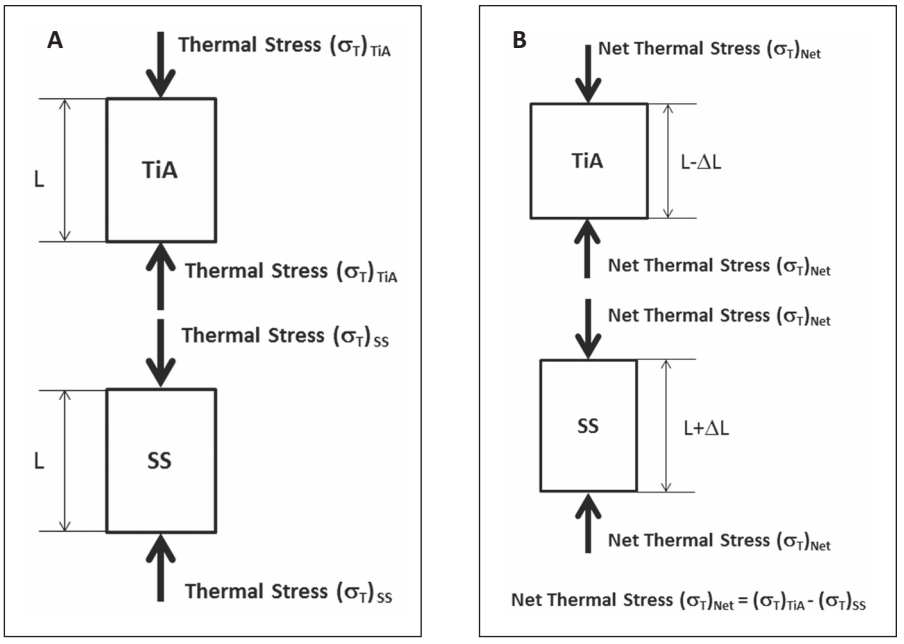

Fig. 11 — Free body diagram of the base materials of DWJs when thermal stresses act at A — 32°C (ambient temperature); B — 750°C (welding temperature).

Mathematically, the slope of the lateral deformation graph (Fig. 5) was in increasing order (Equation 5) with the welding pressure utilized; hence, the lower-range has less slope than the middle-range, and the middle-range has less slope than the higher-range of welding pressure.

$$\text{Welding pressure} \propto \text{lateral deformation of DWJs} \quad (5)$$

And it was also noticed that DWJs fractured at the TiA | Ni interface because the TiA | Ni interface (~750 HV) is much harder than the Ni | SS interface (~330 HV). Consequently, the TiA | Ni interface is more brittle as compared to the Ni | SS interface. In this study, it was also noted that the hardness differences at the TiA | Ni interface (=750 HV–200 HV=550 HV) was higher than that of the hardness difference at the Ni | SS interface (=400 HV–200 HV=200 HV). This observation testified the claim made by Simões et al. (Ref. 38) that DWJs fracture at the interfaces with high hardness differences. The fracture path observations also supported the claim that DWJs fractured along the TiA | Ni interface. This inference was quite consistent with the findings of the reported literature (Refs. 17–19) as well.

Base materials diffusion welded experienced stresses at three successive stages. First, the base materials underwent deformation (purely elastic in nature) due to the static stresses caused by the dead load (welding pressure from 2 to 10 MPa) (Fig. 10A) application just before the furnace was switched 'ON.' Second, the base materials underwent deformation due to increasing dynamic thermal stresses (Fig. 10B) induced due to the linear thermal expansion of the other base materials because of the continuous increase in the furnace temperature from room temperature to the welding temperature (say, 750°C). Thermal stresses reach the maximum value at the welding temperature (750°C). And third, after reaching the designated welding temperature (say, 750°C) the base materials were held at the temperature for 60 min of the welding interval, i.e., during that time onward, the materials were typically subjected to a slowly continuous deformation at constant load (due to welding pressure applied and the thermal stresses induced, see Fig. 10B) at elevated temperatures. This phenomenon is termed as creep (Refs. 39–41).

Of these three stress fields encountered by the materials diffusion welded, the effect of static stresses caused by the dead load was trivial, while the effect of creep phenomenon on the materials diffusion welded was insignificant due to the low order time scale, whereas, the effect of thermal stresses due to

temperature changes had a huge impact on DWJs. Although the thermal stresses encountered by the material were uniformly increasing from the time the furnace was switched 'ON' till the time it reached the welding temperature (750°C).

Thermal stress $(\sigma_T)_{TiA}$ on TiA due to thermal expansion of SS because of temperature change (ΔT) is ~1867.31 MPa (see Appendix), whereas the thermal ((stress) $\sigma_T)_{SS}$ on SS due to thermal expansion of TiA is ~219.70 MPa (see Appendix). To calculate the net thermal stress $(\sigma_T)_{Net}$ acting on the materials, a free body diagram (Fig. 11) of the materials diffusion welded was constructed. As both thermal stresses acting at the interface are opposite in nature, the net thermal stress $((\sigma_T)_{Net} = (\sigma_T)_{TiA} - (\sigma_T)_{SS}$=1867.31 MPa–219.70 MPa) acting on the TiA and SS is ~1647.61 MPa $((\sigma_T)_{Net})$.

Conclusion

This study was performed to know the extent of the influence of welding pressure on the evolution of interfacial microstructure, mechanical properties, and fracture features of solid-state diffusion welded joints of Ti-6Al-4V and 304 stainless steel using 200-μm-thick nickel as an interlayer. DWJs were processed in vacuum at 750°C (welding temperature) for 60 min (welding time) using welding pressure in the range of 2 to 10 MPa in step of 2 MPa. Characterization of the DWJs revealed the following:

1) Interfaces of the DWJs were free from the brittle Fe–Ti-based intermetallics due to the usage of Ni interlayer.

2) Optimal tensile strength of ~560 MPa along with substantial elongation of ~12% was obtained for the DWJs processed at 6-MPa welding pressure considering the minimal lateral deformation of the base metals welded. The tensile strength was more or less flat for the DWJs processed above 6 MPa. Elongation dropped insignificantly for the DWJs processed above 6 MPa.

3) TiA | Ni interface (~750 HV) was much harder than the Ni | SS interface (~330 HV).

4) It was clearly demonstrated that the failure of the DWJs was initiated and propagated specifically at the TiA | Ni interface primarily due to higher hardness difference at the TiA | Ni interface compared to the Ni | SS interface.

5) The fracture surfaces for lower welding pressure (2 MPa) yielded brittle fracture morphologies; whereas the higher welding pressure (8 MPa) yielded mixed mode fractural features.

6) Apart from the welding pressure applied, an additional stress (thermal stress) of ~1647.61 MPa (compressive in nature) was induced on the materials (TiA and SS) diffusion welded due to linear thermal expansion of the materials at the welding temperature (750°C).

Appendix

Considering the materials to be homogeneous and with a uniform cross section throughout the length, stress (σ_T) in any material due to temperature change (ΔT) and the restriction in the linear thermal expansion of another material is given by the following relationship:

$(\sigma_T)_1 = (E_T)_2 (\alpha_T)_2 (\Delta T)$ (Refs. 42, 43)

where
$(\sigma_T)_1$: Thermal stress induced in the material '1' at temperature 'T'

$(E_T)_2$: Young's modulus of material '2' at temperature 'T'
$(\alpha_T)_2$: Coefficient of thermal expansion of the material '2' at temperature 'T'

ΔT: Increase in the temperature

T: Welding temperature (750°C)

T_0: Room temperature (32°C)

so, $\Delta T = T - T_0$=750°C–32°C = 718°C

Case 1: Thermal stress $(\sigma_T)_{TiA}$ on TiA due to thermal expansion of SS because of temperature change (ΔT)

$(\sigma_T)_{TiA} = (E_T)_{SS} \times (\alpha_T)_{SS} \times (\Delta T)$

$(E_T)_{SS}$ = 133.37 GPa (Ref. 44)

$(\alpha_T)_{SS} = 19.5 \times 10^{-6}$ (m/m–°C) (Ref. 45)

so, $(\sigma_T)_{TiA} = 19.5 \times 10^{-6}$ (m/m–°C) × 133.37 GPa × 718°C

so, $(\sigma_T)_{TiA}$= 1867.31 MPa (compressive in nature)

Case 2: Thermal stress $(\sigma_T)_{SS}$ on SS due to thermal expansion of TiA because of temperature change (ΔT)

$(\sigma_T)_{SS} = (E_T)_{TA} (\alpha_T)_{TA} (\Delta T)$

Material properties at higher temperatures are less available in literature, so the authors extrapolated using the available resources at hand.

$(E_T)_{TA}$ < 30 GPa (Ref. 46)
$(\alpha_T)_{TA} = 10.2 \times 10^{-6}$ (m/m–°C) (Ref. 47)
so, $(\sigma_T)_{SS} < 10.2 \times 10^{-6}$ (m/m–°C) × 30 GPa × 718°C

so, $(\sigma_T)_{SS}$ < 219.70 MPa (compressive in nature)

In all of the above calculations, thermal stresses induced in the nickel interlayer due to the expansion of both SS and TiA were not considered for the sake of its negligible thickness (~200 μm) with respect to the thickness of SS and TiA (both ~30 mm).

References

1. Cobb, H. M. 2012. *Dictionary of Metals*. 70, Materials Park, Ohio, ASM International.
2. Banerjee, D., and Williams, J. C. 2013. Perspectives on titanium science and technology. *Acta Materialia* 61: 844–879.
3. Polmear, I. J. 2006. *Light Alloys—from Traditional Alloys to Nanocrystals*. 299–365, 339, Oxford: Butterworth-Heinemann.
4. Yamada, M. 1996. An overview on the development of titanium alloys for non-aerospace application in Japan. *Materials Science and Engineering* 213A: 8–15.
5. McGuire, M. F. 2008. *Stainless Steels for Design Engineers*. 69–90, Materials Park, Ohio, ASM International.
6. Rodin, M. E., Semenov, A. N., Senov, M. I., Plyshevskii, M. I., Novozhilov, S. N., and Rassoshkina, N. S. 2013. Investigations of the strength of steel-titanium diffusion welded joints. *Welding International* 27(6): 482–484.
7. He, P., Yue, X., and Zhang, J. H. 2008. Hot pressing diffusion bonding of a titanium alloy to a stainless steel with an aluminum alloy interlayer. *Materials Science and Engineering* 486A: 171–176.

8. Ghosh, M., Chatterjee, S., and Mishra, B. 2003. The effect of intermetallics on the strength properties of diffusion bonds formed between Ti–5.5Al–2.4V and 304 stainless steel. *Materials Science and Engineering* 363A: 268–274.

9. *http://www.aerospacemetals. com/*

10. Kahraman, N., Gulenc, B., and Findik, F. 2007. Corrosion and mechanical-microstructural aspects of dissimilar joints of Ti–6Al–4V and Al plates. *International Journal of Impact Engineering* 34: 1423–1432.

11. Sun, Z., Annergren, I., Pan, D., and Mai, T. A. 2003. Effect of laser surface remelting on the corrosion behaviour of commercially pure titanium sheet. *Materials Science and Engineering* 345A: 293–300.

12. Zeer, G. M., Zelenkova, E. G., Koroleva, Yu. P., Mikheev, A. A., and Prokopy'ev, S. V. 2013. Diffusion bonding through interlayers. *Welding International* 27(8): 638–643.

13. Hinotani, S., and Ohmori, Y. 1988. The microstructure of diffusion-bonded Ti/Ni interface. *Transactions of the Japan Institute of Metals* 29(2): 116–124.

14. Kundu, S., and Chatterjee, S. 2006. Interfacial microstructure and mechanical properties of diffusion-bonded titanium–stainless steel joints using a nickel interlayer. *Materials Science and Engineering* 425A: 107–113.

15. He, P., Zhang, J., Zhou, R., and Li, X. 1999. Diffusion bonding technology of a titanium alloy to a stainless steel web with an Ni interlayer. *Materials Characterization* 43: 287–292.

16. Kazakov, N. F. 1985. *Diffusion Bonding of Materials*. 11–12, Moscow, Mir Publishers.

17. Thirunavukarasu, G., Kundu, S., Mishra, B., and Chatterjee, S. 2014. Effect of bonding temperature on interfacial reaction and mechanical properties of diffusion-bonded joint between Ti-6Al-4V and 304 stainless steel using nickel as an intermediate material. *Metallurgical and Materials Transactions* 45A: 2067–2077.

18. Thirunavukarasu, G., Kundu, S., Mishra, B., and Chatterjee, S. 2014. Effect of bonding time on interfacial reaction and mechanical properties of diffusion-bonded joint between Ti-6Al-4V and 304 stainless steel using nickel as an intermediate material. *Metallurgical and Materials Transactions* 45A: 2078–2090.

19. Sam, S., Kundu, S., and Chatterjee, S. 2012. Diffusion bonding of titanium alloy to micro-duplex stainless steel using a nickel alloy interlayer: Interface microstructure and strength properties. *Materials and Design* 40: 237–244.

20. Kundu, S., Mishra, B., Olson, D. L., and Chatterjee, S. 2013. Interfacial reactions and strength properties of diffusion bonded joints of Ti64 alloy and 17-4PH stainless steel using nickel alloy interlayer. *Materials and Design* 51: 714–722.

21. Kundu, S., Sam, S., and Chatterjee, S. 2013. Interfacial reactions and strength properties in dissimilar titanium alloy/Ni alloy/microduplex stainless steel diffusion bonded joints. *Materials Science and Engineering* 560A: 288–295.

22. John, V. 1992. I*ntroduction to Engineering Materials,* p. 104, London, Macmillan.

23. Shanmugarajan, B., and Padmanabham, G. 2012. Fusion welding studies using laser on Ti–SS dissimilar combination, *Optics and Lasers in Engineering* 50: 1621–1627.

24. Wang, T., Zhang, B. G., and Feng, J. C. 2014. Influences of different filler metals on electron beam welding of titanium alloy to stainless steel. *Transactions of Nonferrous Metals Society of China* 24: 108–114.

25. Balasubramanian, M. 2015. Development of processing windows for diffusion bonding of Ti–6Al–4V titanium alloy and 304 stainless steel with silver as intermediate layer. *Transactions of Nonferrous Metals Society of China* 25: 2932–2938.

26. Balasubramanian, M. 2016. Characterization of diffusion-bonded titanium alloy and 304 stainless steel with Ag as an interlayer. *The International Journal of Advanced Manufacturing Technology* 82: 153–162.

27. Tomashchuk, I., Sallamand, P., Belyavina, N., and Pilloz, M. 2013. Evolution of microstructures and mechanical properties during dissimilar electron beam welding of titanium alloy to stainless steel via copper interlayer. *Materials Science and Engineering* 585A: 114–122.

28. Norouzi, E., Atapour, M., Shamanian, M., and Allafchian, A. 2016. Effect of bonding temperature on the microstructure and mechanical properties of Ti-6Al-4V to AISI 304 transient liquid phase bonded joint. *Materials and Design* 99: 543–551.

29. Kumar, R., and Balasubramanian, M. 2015. Experimental investigation of Ti–6Al–4V titanium alloy and 304L stainless steel friction welded with copper interlayer. *Defence Technology* 11: 65–75.

30. Fischer, T. 2009. *Materials Science for Engineering Students*. 97, 19–21, 112–115, San Diego, Academic Press.

31. Porter, D. A., Easterling, K. E., and Sherif, M. Y. 2009. *Phase Transformations in Metals and Alloys*. 65, 7–9, 100–104, Boca Raton, CRC.

32. Jr Messler, R. W. 2011. *The Essence of Materials for Engineers*. 307–308, Burlington, Massachusetts: Jones & Bartlett.

33. Dieter, G. E. 1988. *Mechanical Metallurgy.* 231–233, Singapore, McGraw-Hill.

34. Kelly, P. F. 2015. *Properties of Materials*. 7–12, Boca Raton, CRC.

35. White, M. A. 2012. *Physical Properties of Materials*. 383–394, Boca Raton, CRC.

36. Lovell, M. C., Avery, A. J., and Vernon, M. W. 1984. *Physical Properties of Materials*. 87–92, Wokingham, Berkshire, UK, Van Nostrand Reinhold.

37. Brandes, E. A., and Brook, G. B. 1992. *Smithells Metals Reference Book*. 15–3, Oxford, Butterworth-Heinemann.

38. Simões, S., Viana, F., Koçak, M., Ramos, A. S., Vieira, M. T., and Vieira, M. F. 2011. Diffusion bonding of TiAl using reactive Ni/Al nanolayers and Ti and Ni foils. *Materials Chemistry and Physics* 128: 202–207.

39. Gottstein, G. 2007. *Physical Foundations of Materials Science*. 281–282, New Delhi, Springer.

40. Finnie, I., and Heller, W. R. 1959. *Creep of Engineering Materials*. 16, New York, McGraw-Hill.

41. Hetnarski, R. B., and Eslami, M. R. *Thermal Stresses—Advanced Theory and Applications*. 499–510, Springer.

42. Beer, F. P., Jr Johnston, E. R., and DeWolf, J. T. 2006. *Mechanics of Materials*. 74–75, New Delhi, Tata McGraw-Hill.

43. Srinath, L. S., Desayi, P., Murthy, N. S., and Ramu, S. A. 2001. *Strength of Materials*. 60–61,New Delhi, Macmillan India.

44. *http://bssa.org.uk/topics.php?article=139*.

45. *http://asm.matweb.com/search/SpecificMaterial.asp?bassnum=MQ304A*

46. Veiga, C., Davim, J. P., and Loureiro, A. J. R. 2012. Properties and applications of titanium alloys: A brief review. *Reviews on Advanced Materials Science* 32: 133–148.

47. *http://asm.matweb.com/search/SpecificMaterial.asp?bassnum=MTP641*.